



Predicting the Density of Solid and Liquid Near-Eutectic Ga–In–Sn Alloy

Matthias H. Buschmann¹

Received: 1 November 2023 / Accepted: 10 November 2023 / Published online: 18 December 2023
© The Author(s), under exclusive licence to Springer Science+Business Media, LLC, part of Springer Nature 2023

Abstract

Europe has set itself the goal of reducing net greenhouse gas emissions to zero by 2050. This requires innovative concepts for the transfer of thermal energy. One of these could be the use of liquid metals and alloys as heat carriers. For this purpose, the precise knowledge of the thermophysical properties of these materials is of great importance. This study therefore aims to model the temperature dependent density of solid and liquid near-eutectic gallium-indium-tin alloys. Three approaches—weighted fitting of experimental data, modelling based on atomic volumes of alloying elements, and an approach that accounts for possible excess density—are utilised. Details of these strategies with respect to the thermophysical properties of the alloying elements, and the binary sub-alloys, are discussed. The resulting correlations are validated using six independent experimental data sets. The study concludes that, currently, the fitting polynomials are the most reliable models. The estimates based on atomic volumes are in close agreement with these functions. This is true for both the solid and liquid states. This marks the first time that the density of the solid state of this particular alloy has been modelled. The difficulties associated with modelling the density excess are manifold. This includes the lack of precise thermophysical properties for the alloying elements. The study paves the way for near-eutectic liquid gallium-indium-tin alloy as a heat carrier. In the view of the potential importance of heat transfer employing liquid metals, these findings highlight the need for further investigations in this field.

Keywords Density · Excess · Modelling · Near-eutectic Ga–In–Sn alloy

Abbreviations

c_p	Isobaric heat capacity [$\text{J}\cdot\text{kg}^{-1}\cdot\text{K}^{-1}$]
G	Gibbs energy: [J]
H	Enthalpy of mixing [$\text{J}\cdot\text{mol}^{-1}$]

✉ Matthias H. Buschmann
Matthias.Buschmann@ilkdresden.de

¹ Institut für Luft- und Kältetechnik gGmbH Dresden, 01309 Dresden, Germany

L_{xy}	Interaction parameters [$\text{J}\cdot\text{mol}^{-1}$]
T	Temperature [K]
V_i	Atomic volume of component i [$\text{m}^3\cdot\text{mol}^{-1}$]
X_i	Molar fraction of component i [-]
β	Expansion coefficient [K^{-1}]
ρ	Density [$\text{kg}\cdot\text{m}^{-3}$]

Subscripts

EGaInSn	Near-eutectic gallium-indium-tin alloy
eu	Eutectic
fit	Fitting approach
Ga	Gallium
GaIn	Binary gallium indium alloy
GaSn	Binary gallium tin alloy
In	Indium
InSn	Binary indium tin alloy
liq	Liquid
m	Melting
Sn	Tin
sol	Solid

Superscripts

exc	Excess
$i\dots 0, 1$	Constant and linear interaction parameters

1 Introduction

Europe's Green Deal released in 2019/20 [1] aims to decrease the net greenhouse gas emissions in the European Union to zero by 2050. In addition to reducing the consumption of fossil fuels, this requires new and innovative approaches to thermal energy. One such approach could be the use of liquid metals for heat transfer [2]. Knowledge of the thermophysical properties, both in the solid and liquid state of the metals and their alloys, is of utmost importance for the correct design and operation of corresponding devices.

For heat transfer applications, the focus is on metals with a low melting point. This includes, in particular, gallium. Among the advantages of this boron group, metal, and its alloys with indium and tin compared to mercury and sodium is their low level of toxicity and the non-flammability. Furthermore, the vapour pressure is significantly lower than that of, e.g., mercury. Gallium-based alloys show outstanding high electrical and thermal conductivity combined with low viscosity. Because of pure gallium's already low melting point of 29.76 °C (302.91 K), all of its alloys are likely to have even lower melting points. Therefore, especially the ternary eutectic of gallium, indium, and tin has a large field of applications. They range from sensor technology [3] to flexible electronics [4] and heat transfer [5]. Hao et al. [6] and

Riehl and Buschmann [7] investigate, for example, oscillating heat pipes operated with an emulsion of this specific alloy and water.

This study is part of a joint theoretical and experimental effort to investigate the thermophysical properties of the ternary eutectic gallium-indium-tin alloy [8, 9]. The focus is on the temperature dependent density of the liquid and solid alloy. Three approaches model this parameter. Based on experimental data available in the open literature, error weighted fitting functions are derived. A second approach models the density based on the atomic volumes of the alloying elements. Finally, the study presents a modelling strategy considering a possible density excess. An evaluation of the results of the study provides recommendations for application as well as for further research tasks.

2 The Near-Eutectic Ga–In–Sn Alloy

Figure 1 shows three samples of the near-eutectic Ga–In–Sn alloy. While the use of tin dates back to 5000 BC, the elements indium and gallium were not identified until the end of the nineteenth century. Paul Émile Lecoq de Boisbaudran, the discoverer of gallium, was probably the first to experiment with gallium-indium alloys [10]. Early analyses of the ternary near-eutectic Ga–In–Sn alloy can be found in reports by Spengler [11] in the middle of the last century.

Spengler [11] already mentions that, due to the strong capability of subcooling of the alloy, the melting temperature could not be determined exactly. Evans and Prince [12] conduct a thorough thermal analysis of the Ga–In–Sn system, determining the liquidus and characterising the reactions of the system. They report a eutectic

Fig. 1 Liquid near-eutectic Ga–In–Sn alloy. The photo shows the testing of aluminium, copper, and stainless steel samples for corrosion

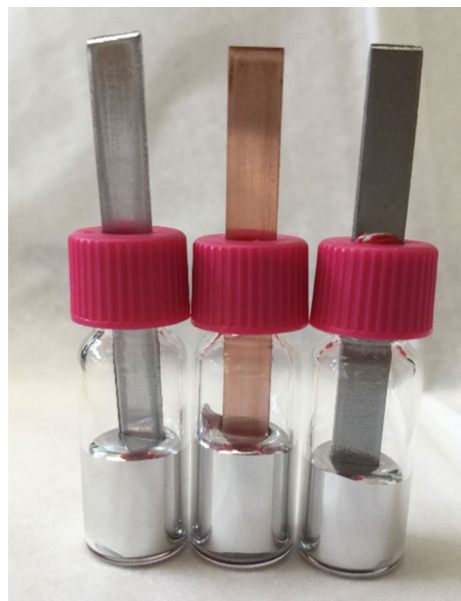


Table 1 References for experimental density data

Reference and symbol in following diagrams	Employed alloy as given by the authors Ga/In/Sn	Measurement apparatuses	Experimental error
Prokhorenko et al. [15] ▶	67.0/20.5/12.5 wt.% 77.3/14.4/8.3 at.%	quartz pycnometer	$< \pm 0.50\%$
Migai et al. [16] ◀	67.0/20.5/12.5 wt.% 77.2/14.3/8.4 at.%	buoyancy method	NA
Plevachuk et al. [17] ▲	67.0/20.5/12.5 wt.% 77.2/14.4/8.4 at.%	large drop method, which is a modification of the sessile drop method	$\pm 1.50\%$
Wang et al. [18] ▼	68.8/19.2/12.0 wt.% 78.8/13.2/8.0 at.%	Netzsch DIL 402C pushrod dilatometer	NA
Laube et al. [19] ◆	65.9/20.3/13.8 wt.% 76.3/14.3/9.4 at.%	pycnometer ISO 3507 design 3 Gay-Lussac, Brand	$\pm 0.06\%$
Geratherm [20] ★	NA	NA	NA

Italics indicate predicted values. All other values are taken directly from the original publications

temperature of $10.7\text{ }^{\circ}\text{C} \pm 0.3\text{ K}$ ($283.85 \pm 0.3\text{ K}$) and identify the ternary eutectic as 66.0 wt.% Ga, 20.5 wt.% In, and 13.5 wt.% Sn (76.4/14.4/9.2 at.%). Most experimentalists today work with alloys very close to this mixture (Table 1) and consider the melting point found in [12]. Figure 2 shows the melting points of the alloying partners Ga, In, and Sn, the eutectic binary sub-alloys GaIn, GaSn, and InSn, as well as that of the ternary eutectic.

Recent literature reveals a 20 K gap between solidification and melting [13]. According to these studies, crystallisation occurs below $-10\text{ }^{\circ}\text{C}$ (263.15 K) and may not be complete until $-30\text{ }^{\circ}\text{C}$ (243.15 K). In addition, the solidification and melting processes may well depend on the heating or cooling rates. Furthermore, even small impurities from elements like zinc may affect thermophysical properties, including the melting point [14]. Due to these imponderables, the melting point and mixture provided by Evans and Prince [12] are understood as the nominal parameters of the *near-eutectic Ga–In–Sn alloy*. This strategy also allows the use of averaging over the small discrepancies of the different alloy mixtures used for the experiments.

2.1 Experimental Density Data

Table 1 compiles the experimental data employed (Fig. 3). Only one study with eight values provides data for the solid state [20]. The total number of investigations, six, with a total of 78 values, is significantly larger. Unfortunately, only for three

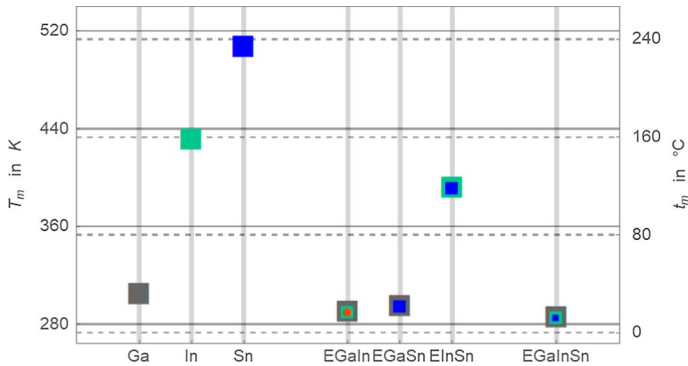


Fig. 2 Melting points of gallium, indium, and tin [21], the binary eutectic sub-alloys GaIn, GaSn [22], InSn [23], and the near-eutectic Ga–In–Sn alloy [12]. The red dot indicates the melting temperatures found by Boisbaudran [10] for GaIn alloys

data sets [15, 17, 19] is the experimental error provided. Moreover, the employed measurement techniques to obtain the data differ. Two studies use pycnometers [15, 19] and one uses a buoyancy method [16]. One attempt employs a modified sessile drop method [17], while another uses a commercial pushrod dilatometer [18].

Migai et al. [16] and Plevachuk et al. [17] are the only references that provide explicit correlations for the liquid density of the near-eutectic Ga–In–Sn alloy. Both equations show a linear dependence on temperature. The Plevachuk correlation additionally refers to the melting temperature of the alloy. The value T_m = of 283.7 K is very close to the value of Evans and Prince [12].

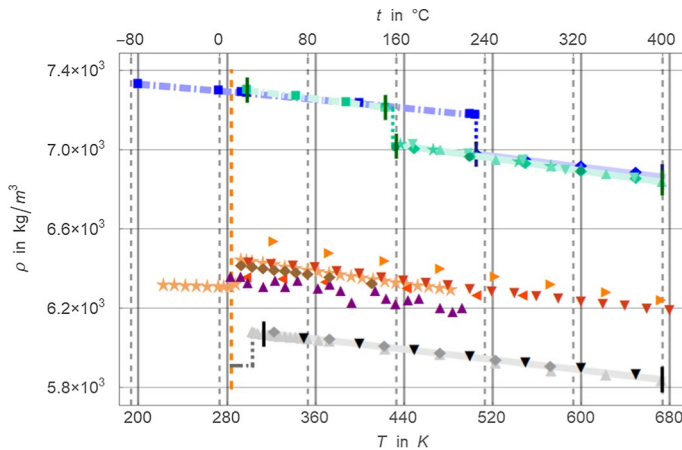


Fig. 3 Experimental density data of near-eutectic Ga–In–Sn alloy in comparison with the densities of the alloying components. Symbols for near-eutectic Ga–In–Sn alloy as given in Table 1. Vertical broken orange line identifies the melting point of near-eutectic Ga–In–Sn alloy. Symbols and curves are grey for Gallium, green for indium, and blue for tin. Short vertical grey, green, and blue lines indicate fitting regions of Ga, In, and Sn data, respectively

3 Modelling Strategies

This study explores three strategies either to fit or to model the density of the solid and liquid near-eutectic Ga–In–Sn alloy. First, the available experimental data are approximated employing a weighted fitting approach. Second, the density is estimated based on the atomic volumes of the alloying partners. Third, a prediction is made of the alloy density based on the properties of the constituent elements and the enthalpy of mixing of the system.

While the first and the second approaches hypothesise that the alloy does not have an excess due to the mixing of dissimilar atoms, the third method attempts to include such an effect. None of the strategies consider a pressure dependency. Comparison of the results with experimental data validates the different modelling strategies. For all predictions, MATHEMATICA 13.3 is used.

3.1 Weighted Fitting Approach

Because the experimental errors of the data for the liquid alloy differ by almost three orders of magnitude (e.g. 0.06% [19] to 1.50% [17]), an error weighted fitting strategy is employed. Inspired by Plevachuk et al. [17], polynomials are used for the correlations.

$$\rho_{\text{fit,EGaInSn}}(T) = \sum_{i=0}^n \rho_i (T - T_{\text{m,EGaInSn}})^i \quad (1)$$

3.1.1 Solid Alloy

For the solid state, the fitting does not use a weighting. The reason is simply that the only available data set [20] does not provide such information. Eight data points ranging from 223.15 to 283.15 K (-50 to 10 °C) are used. The fitting function for the solid state with $n=2$ is:

$$\begin{aligned} \rho_{\text{sol,fit,EGaInSn}}(T) = & 6304.30 \frac{\text{kg}}{\text{m}^3} + 4.29 * 10^{-2} \frac{\text{kg}}{\text{m}^3} \frac{1}{\text{K}} (T - T_{\text{m,EGaInSn}}) \\ & + 1.85 * 10^{-3} \frac{\text{kg}}{\text{m}^3} \frac{1}{\text{K}^2} (T - T_{\text{m,EGaInSn}})^2 \quad R^2 = 1 \end{aligned} \quad (2)$$

Were $T_{\text{m,EGaInSn}}$ denotes the nominal melting point of the near-eutectic Ga–In–Sn alloy at 283.85 K (10.7 °C). All experimental data lay in an error band of $\pm 0.25\%$ (Fig. 4). The standard errors of the parameters of Eq. 2 are $\pm 0.28 \text{ kg}/\text{m}^3$, $\pm 2.42 * 10^{-2} \text{ kg}/(\text{m}^3 \text{ K})$ and $\pm 3.90 * 10^{-4} \text{ kg}/(\text{m}^3 \text{ K}^2)$.

3.1.2 Liquid Alloy

For the fitting, the three data sets with known experimental error are selected [15, 17, 19]. The reciprocal of the squares of the experimental errors serve as weights.

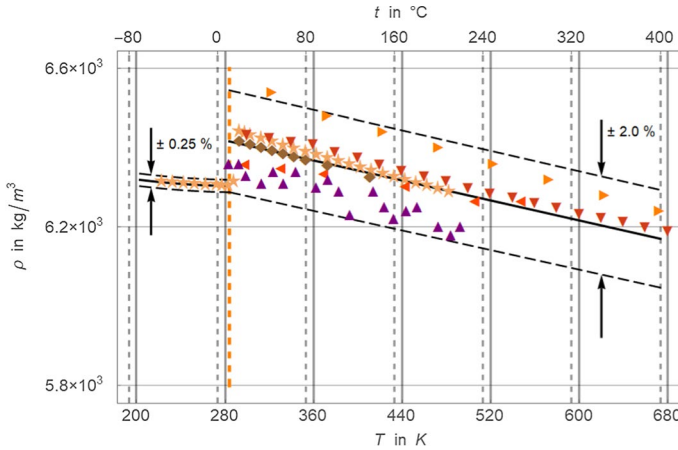


Fig. 4 Quadratic fit of solid density Eq. 2 and weighted linear fit of liquid density data Eq. 3. Broken curves show intervals that cover all data

The fit considers altogether 36 data points ranging from 283.7 to 673.0 K (10.7 to 400.0 °C).

For $n = 1$ the correlation reads:

$$\rho_{\text{liq,fit,EGaInSn}}(T) = 6417.02 \frac{\text{kg}}{\text{m}^3} + 0.6320 \frac{\text{kg}}{\text{m}^3} \frac{1}{\text{K}} (T - T_{\text{m,EGaInSn}}) \quad R^2 = 0.9999 \tag{3}$$

All experimental data including those that are not used for the fitting [16, 18] lay in an error band of $\pm 2\%$ (Fig. 4). When considering only the more recent data [18–20], the error band reduces to $\pm 1\%$ (Fig. 5). The standard errors of the parameters of Eq. 3 are $\pm 3.87 \text{ kg/m}^3$ and $\pm 0.06 \text{ kg}/(\text{m}^3 \text{ K})$.

The equivalent parameters of the Plevachuk-correlation [17] are 6360.0 kg/m^3 for the density at the melting point and $0.7760 \text{ kg}/(\text{m}^3 \text{ K})$ for the density temperature coefficient. With less than 1% difference, the constant is in excellent agreement with Eq. 3. Similarly, the difference between the constant given by Migai et al. [16] Eq. 2 is less than 1.2%. However, the density temperature coefficient of the Plevachuk-correlation is about 22% higher. In other words, this regression line has a steeper slope.

Increasing n to 2 or 3 does not improve the fit. The R^2 values are identical to that of Eq. 3. The standard errors for the first two parameters of these polynomials are with $\pm 4.37 \text{ kg/m}^3 / \pm 3.94 \text{ kg/m}^3$ and $\pm 0.10 \text{ kg}/(\text{m}^3 \text{ K}) / \pm 0.06 \text{ kg}/(\text{m}^3 \text{ K})$, respectively, comparable.

3.2 Modelling Based on the Atomic Volumes of the Alloying Elements Strategies

The first modelling estimation is based on the linear combination of the atomic volumes V_i of the pure constituent elements weighted with their molar fractions X_i [24, 25]

$$\overline{V_{\text{EGaInSn}}(T)} = X_{\text{Ga}} V_{\text{Ga}}(T) + X_{\text{In}} V_{\text{In}}(T) + X_{\text{Sn}} V_{\text{Sn}}(T) \quad (4)$$

and for the density

$$\frac{1}{\overline{\rho_{\text{EGaInSn}}(T)}} = \frac{X_{\text{Ga}}}{\rho_{\text{Ga}}(T)} + \frac{X_{\text{In}}}{\rho_{\text{In}}(T)} + \frac{X_{\text{Sn}}}{\rho_{\text{Sn}}(T)} \quad (5)$$

In the following, correlations for the solid and liquid densities of the alloying partners' gallium, indium, and tin are presented, focussing on the temperature range of the available experimental data of the near-eutectic Ga–In–Sn alloy. These functions utilise recommended and experimental data as well as data resulting from molecular dynamics simulations.

3.2.1 Solid Alloy

Equation (5) applies readily to the solid phase since the pure constituents are all solid below the melting point of the alloy. For this, the densities of solid gallium, indium, and tin must be available.

To the best of the author's knowledge, almost no density data are published for gallium below its melting point of 302.91 K (29.76 °C). Therefore, the value of 5.910 kg/m³ given in the CRC Handbook [21] for 298.15 K (25 °C) is assumed for the entire temperature range considered.

The density correlation for solid indium results from a linear fit of the data by Williams and Miller [26] and from the experimental data point by Wang et al. [27] for 423.15 K (150 °C). Therewith altogether five data points in the range from 298.15 to 423.15 K (25 to 150 °C) are considered. The correlation reads:

$$\rho_{\text{sol,fit,In}}(T) = 7211.1 \frac{\text{kg}}{\text{m}^3} - 0.6984 \frac{\text{kg}}{\text{m}^3} \frac{1}{\text{K}} (T - T_{\text{m,In}}) \quad R^2 = 1 \quad (6)$$

The standard errors of the parameters are $\pm 2.26 \text{ kg/m}^3$ and $\pm 0.03 \text{ kg}/(\text{m}^3 \text{ K})$. The melting point of indium $T_{\text{m,In}}$ is 429.75 K (156.60 °C).

Stankus and Khairulin [28] provide a correlation for the density of solid tin:

$$\begin{aligned} \rho_{\text{sol,fit,Sn}}(T) &= 7289.8 \frac{\text{kg}}{\text{m}^3} - 0.4853 \frac{\text{kg}}{\text{m}^3} \frac{1}{\text{K}} (T - T_{\text{m,Sn}}) \\ &\quad - 2.41866 \times 10^{-4} \frac{\text{kg}}{\text{m}^3} \frac{1}{\text{K}} (T - T_{\text{m,Sn}})^2 \quad (7) \\ &293\text{K} < T < T_{\text{m,Sn}} \end{aligned}$$

Here, $T_{\text{m,Sn}}$ denotes the melting point of tin with 505.08 K (231.93 °C).

Employing the mass concentrations proposed by Evans & Prince [12] for the solid near-eutectic Ga–In–Sn alloy, Eq. 5 yields a circumstantial correlation for $\overline{\rho_{\text{sol,EGaInSn}}(T)}$ consisting of a fraction whose numerator and denominator each consist of a fourth order polynomial. For simplification, a first-order series expansion of the above equation is performed. The resulting correlation reads:

$$\overline{\rho_{\text{sol,EGalnSn}}(T)} = 6305.83 - 0.1490(T - T_{\text{m,EGalnSn}}) \quad (8)$$

The difference between Eq. 8 and the correlation following straight from (5) is less than 0.004% throughout the range of interest (223.15 to 283.15 K). Figure 5 shows that the experimental data [20] are covered within an error band of $\leq \pm 0.25\%$. Moreover, the fitting function (1) and Eq. 8 show nearly identical results, indicating the applicability of the atomic volume-based strategy for the solid alloy.

3.2.2 Liquid Alloy

The melting points of gallium, indium, and tin are significantly higher than the nominal melting point of the near-eutectic Ga–In–Sn alloy at 283.85 K. Consequently, Eq. 5 delivers a reliable result for only above the melting point of tin. However, extrapolating the determined correlation to close the remaining temperature interval is possible, but its validity must be proven employing experimental data.

The density correlation of liquid gallium is based on the data recommended by Assael et al. [29] and the experimental data provided by Kezik et al. [30] and Ayrinhac et al. [31]. Altogether 30 data points in the range from 313.15 to 673.15 K (40 to 400 °C) are considered. The resulting correlation reads:

$$\rho_{\text{liq,fit,Ga}}(T) = 6082.84 \frac{\text{kg}}{\text{m}^3} - 0.6555 \frac{\text{kg}}{\text{m}^3} \frac{1}{\text{K}} (T - T_{\text{m,Ga}}) \quad R^2 = 0.9999 \quad (9)$$

The standard errors of the parameters are $\pm 1.44 \text{ kg/m}^3$ and $\pm 0.0082 \text{ kg}/(\text{m}^3 \text{ K})$.

The fit of the density of liquid indium is based on the data recommended by Assael et al. [29] and the experimental data provided by Williams and Miller [26] and Wang et al. [27]. Additionally, results from the molecular dynamic simulation by Belashchenko [32] are employed. A total of 23 values in the range from 400.00 to 673.15 K (159.85 to 400.00 °C) are considered. The correlation reads:

$$\rho_{\text{liq,fit,In}}(T) = 7030.03 \frac{\text{kg}}{\text{m}^3} - 0.7872 \frac{\text{kg}}{\text{m}^3} \frac{1}{\text{K}} (T - T_{\text{m,In}}) \quad R^2 = 0.9999 \quad (10)$$

The standard errors of the parameters are $\pm 2.30 \text{ kg/m}^3$ and $\pm 0.0176 \text{ kg}/(\text{m}^3 \text{ K})$.

The fit of the density of liquid tin is based on the data recommended by Assael et al. [33] and the experimental data provided by Stankus & Khairulin [28]. Eight data points in the range from 505.08 to 700.00 K (231.91 to 426.85 °C) are considered. The correlation reads:

$$\rho_{\text{liq,fit,Sn}}(T) = 6980.54 \frac{\text{kg}}{\text{m}^3} - 0.6881 \frac{\text{kg}}{\text{m}^3} \frac{1}{\text{K}} (T - T_{\text{m,Sn}}) \quad R^2 = 1 \quad (11)$$

The standard errors of the parameters are $\pm 2.75 \text{ kg/m}^3$ and $\pm 0.0228 \text{ kg}/(\text{m}^3 \text{ K})$.

Equations (8–10) are in excellent agreement with the density correlations for liquid gallium and indium [29, 33].

Again, the composite proposed by Evans & Prince [12] for the near-eutectic Ga–In–Sn alloy is employed to derive the density correlation:

$$\overline{\rho_{\text{liq,EGaInSn}}(T)} = 6403.22 \frac{\text{kg}}{\text{m}^3} - 0.6827 \frac{\text{kg}}{\text{m}^3} \frac{1}{\text{K}} (T - T_{\text{m,EGaInSn}}) \quad (12)$$

Figure 5 shows the extrapolation of Eq. 12 toward $T_{\text{m,EGaInSn}}$ in relation to experimental data and to the results of the weighted fit Eq. 3. Up to 373.15 K (100°C), the difference between both equations is about 0.3%, which is mainly caused by a 0.22% lower constant of (12).

Gallium's density increase from the solid to the liquid state is clearly visible in Fig. 5. The near-eutectic Ga–In–Sn alloy shows a similar effect. For gallium, this density jump amounts to approximately 3%. Employing the only data set crossing the melting point [20], the experimental density jump of the near-eutectic Ga–In–Sn alloy is about 2.16%.

The value for the density jump obtained from the fitting functions (1) and (3) exactly at $T_{\text{m,EGaInSn}}$ is 1.80%, and from the estimations based on atomic volumes Eqs. 8, 12 1.54%. It seems plausible that for the alloy the effect is mainly caused by its high gallium content. However, it is of course smaller than for pure gallium.

Figure 6 represents Eq. 12 in the entire range of the available data for the liquid alloy. The difference to the fitting function (3) grows with increasing temperature and reaches about -0.55% at $T=673.15$ K. The reason for this is mainly the steeper slope of Eq. 12. Nevertheless, Eq. 12 always falls within the $\pm 1\%$ error band of the fitting function (3). Furthermore, all experimental data except the four lowest temperature values of [15] are within the $\pm 2\%$ error range. This again underpins the

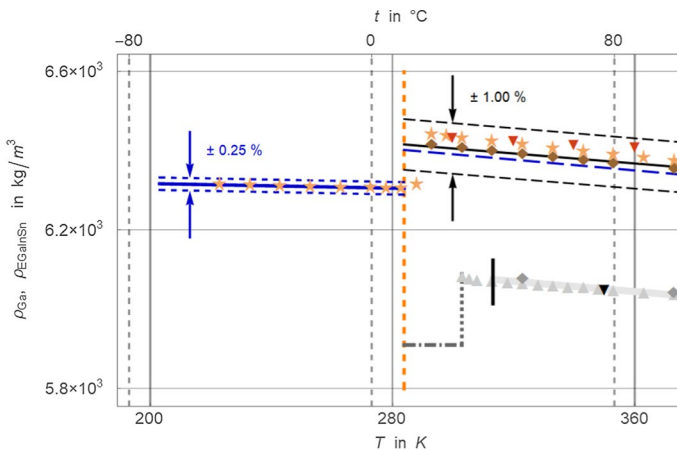


Fig. 5 Modelling of solid and liquid density based on atomic volumes of the alloying elements. Full black line indicates linear fit Eq. 3 $\pm 1\%$. Blue line (left to melting temperature) indicates modelling of solid alloy according to Eq. 8 $\pm 0.25\%$. Blue broken line (right to melting temperature) indicates extrapolation of Eq. 12 for the liquid alloy

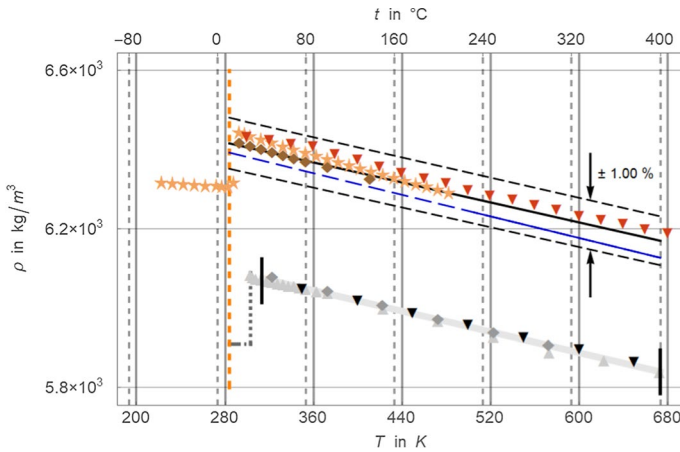


Fig. 6 Modelling of liquid density of near eutectic Ga–In–Sn alloy based on the atomic volumes of the alloying elements. Full black line indicates linear fit Eq. 3 ± 1%. Blue line indicates modelling Eq. 12

applicability of the atomic volume-based strategy for predicting the density of the near-eutectic Ga–In–Sn alloy.

3.3 Modelling Including Excess

3.3.1 Model Approach

Caused by the inequality of the alloying metal atoms, a change in atomic bonding and structuring may accompany the formation of alloys. This atomic disparity leads to modifications in the interatomic distance and thus to differences in the atomic packing density [34]. Therefore, the real, experimentally confirmed densities often differ from the correlations resulting from Eqs. 4–5. This deviation is the temperature dependent excess volume $\Delta V_{EGaInSn}^{exc}(T)$.

Predel and Emam [35] already point out that probably all three, the excess density, the excess enthalpy, and the excess entropy, are correlated. In a more recent study, Liu et al. [34] relate the molar volume $V_{EGaInSn}(T)$ and the enthalpy of mixing $\Delta H_{EGaInSn}^{exc}(T)$. Their main argument – although there exists no direct link between these two properties – is that both properties depend on the temperature.

$$V_{EGaInSn}(T) = \overline{V_{EGaInSn}(T)} * Exp[\Lambda_{EGaInSn}(T) * \Delta H_{EGaInSn}^{exc}(T)] \tag{13}$$

The coefficient $\Lambda_{EGaInSn}(T)$ is the molar mean of the ratios of the thermal expansion coefficients $\beta_i(T)$ at constant pressure and the isobaric heat capacities $c_{p,i}(T)$ of the near-eutectic Ga–In–Sn alloy’s constituents

$$\Lambda_{EGaInSn}(T) = X_{Ga} \frac{\beta_{Ga}}{c_{p,Ga}} + X_{In} \frac{\beta_{In}}{c_{p,In}} + X_{Sn} \frac{\beta_{Sn}}{c_{p,Sn}} \tag{14}$$

The enthalpy of mixing $\Delta H_{EGaInSn}^{exc}$ follows from the Gibbs excess energy according to

$$\Delta H_{EGaInSn}^{exc} = \Delta G_{EGaInSn}^{exc} - T \frac{d\Delta G_{EGaInSn}^{exc}}{dT} \tag{15}$$

Gibbs excess energy of the near-eutectic Ga–In–Sn alloy is the sum of the contributions $\sum \Delta G_{binary}^{exc}$ of the binary sub-alloys GaIn, GaSn, and InSn and a ternary component $\Delta G_{ternary}^{exc}$ that represents the interaction of the atoms of the alloying constituents.

$$\Delta G_{EGaInSn}^{exc} = \sum \Delta G_{binary}^{exc} + \Delta G_{ternary}^{exc} \tag{16a}$$

$$\sum \Delta G_{binary}^{exc} = \Delta G_{GaIn}^{exc} + \Delta G_{GaSn}^{exc} + \Delta G_{InSn}^{exc} \tag{16b}$$

$$\sum \Delta G_{ternary}^{exc} = X_{Ga} X_{In} X_{Sn} [X_{Ga} L_{GaInSn}^0 + X_{In} L_{GaInSn}^1 + X_{Sn} L_{GaInSn}^2] \tag{16c}$$

where L_{GaInSn}^i denote the interaction parameters of the ternary system.

Series expansions with the corresponding Redlich–Kister coefficients $L_{XY}^i(T)$ represent the excess energies of the three binary sub-alloys.

$$\Delta G_{XY}^{exc} = X_X X_Y \sum_{i=0}^2 L_{XY}^i(T) (X_X - X_Y)^i \text{ with } XY \dots \text{ GaIn, GaSn and InSn} \tag{17}$$

To the best of the author’s knowledge, the interaction parameters needed to solve Eq. 16c are not available in the open literature. Consequently, Eq. 16c is bolstered subsidised by a geometrical model for ternary alloys [36]. The general idea of geometrical models is to predict the density of the ternary near-eutectic Ga–In–Sn alloy based on its binary sub-alloys. The approach is

$$\Delta G_{ternary}^{exc} = \sum \omega_{XY} \Delta G_{XY}^{exc} \text{ with } \omega_{XY} = \frac{X_X X_Y}{X_{X(XY)} X_{Y(XY)}} \tag{18}$$

where ΔG_{XY}^{exc} denotes the excess densities of the binary sub-alloys. The weighting functions ω_{XY} are predicted from the molar fractions X_X and X_Y of the ternary near-eutectic Ga–In–Sn alloy and the molar fractions $X_{X(XY)}$ and $X_{Y(XY)}$ of the constituents X and Y of the binary alloy XY. Here X, Y, and Z stand for Ga, In, and Sn, respectively.

Unfortunately, this strategy is not applicable to the density of the solid state of the investigated alloy. The reason for this is that neither sufficient information for the thermal expansion coefficients nor for the heat capacity are available for the binary sub-alloys.

3.3.2 Thermal Expansion Coefficient and Isobaric Heat Capacity of Alloying Partners

To follow the approach outlined above, the thermal expansion coefficients and the heat capacities of the alloy constituents must be available. The first thermophysical properties result directly from the density correlations for gallium, indium, and tin (9–11) according to

$$\beta(T) = -\frac{1}{\rho} \left(\frac{\partial \rho}{\partial T} \right)_p \quad (19)$$

with

$$\beta_{\text{liq,Ga}}(T) = (9582.7 - T)^{-1}, \beta_{\text{liq,In}}(T) = (9359.6 - T)^{-1}, \quad (20)$$

$$\beta_{\text{liq,Sn}}(T) = (10649.5 - T)^{-1}$$

The NIST Chemistry WebBOOK, SRD 69 [37] provides a correlation for gallium's liquid phase heat capacity (Shomate equation), which is as follows:

$$c_{p,\text{liq,Ga}}(T) = 14.3425(24.6214 + \frac{286145.0}{T} + 2.7014 * 10^{-3}T - 1.2721 * 10^{-6}T^2 + 1.9652 * 10^{-10}T^3) \quad (21)$$

A fit of the data provided by the Indium Cooperation [38] delivers the heat capacity correlation for liquid indium

$$c_{p,\text{liq,In}}(T) = 264.5700 - 2.1829 * 10^{-2}T + 9.6512 * 10^{-6}T^2 \quad (22)$$

Finally, for liquid tin we use the heat capacity correlation mentioned by Sharafat and Ghoniem [39].

$$c_{p,\text{liq,Sn}}(T) = 351.6334 - 3.227 * 10^{-1}T + 2.2925 * 10^{-4}T^2 \quad (23)$$

3.3.3 Density of Binary Sub-alloys

Tables 2 and 3 compile characteristic parameters and the interaction parameters $L_{XY}^i(T)$ for the liquid phase of the binary sub-alloys GaIn, GaSn, and InSn. In all cases, these parameters are equal to zero for $i > 1$. Based on the interaction parameters employing Eqs. 4, 13–17, the temperature- and concentration-dependent density and density excess functions are predicted. Experimental data (Table 2) serve for the validation of the obtained correlations. Table 3 compiles the interaction parameters and enthalpy of mixing correlations for the liquid phase of the binary sub-alloys. Table 4 gathers the maximal excess and the density excess of the eutectic binary sub-alloys.

Employing two independent sets of interaction coefficients [49, 50] and an enthalpy of mixing correlation [51], the density excess of liquid Galn is described.

Table 2 Characteristics and experimental databases of the binary sub-alloys GaIn, GaSn, and InSn

Binary sub-alloy	Binary sub-alloy		Experimental data references and symbols
	Eutectic composite	$T_{eu,m}$	
GaIn	Ga 78.6/In 21.4 wt% ^a <i>85.1/21.4 at. %</i>	288.85 K ^b (15.56 °C)	323 K: ★ ^c , ★ ^d , ★ ^e 573 K: ■ ^c , ■ ^e , ■ ^f
GaSn	Ga 86.3/In 13.7 wt% ^a <i>91.5/8.8 at. %</i>	293.63 K ^b (20.48 °C)	573 K: ■ ^f , ■ ^g , ■ ^h
InSn	In 49.1/Sn 50.9 wt% ^{a,i} <i>49.9/50.1 at. %</i>	390.15 K ^j (117.00 °C)	523 K: ■ ^k , ■ ^l , ■ ^l fitting function $f(T, X_{In})^m$

Italics indicate predicted values. All other values are taken directly from the original publications

^aEvans and Prince [12]

^bBurdakin et al. [22]

^cYu et al. [40]

^dXu et al. [41]

^eProkhorenko et al. [42]

^fPredel and Emam [43]

^gGancarz [44]

^hKattner [45]

ⁱStankus et al. [46]

^jOrr et al. [23]

^kPstruś [47]

^lMoser et al. [48]

^mBerthou and Tougas [49]

Table 3 Interaction parameters and enthalpy of mixing correlations for the liquid phase of the binary sub-alloys

Binary alloy	L_{XY}^0, L_{XY}^1 and ΔH_{XY}^{exc}		Colours and references
GaIn	4573.532	- 36.315	— [50]
	4450 + 1.19185 (T/K)	0.25943 (T/K)	— [51]
	$\Delta H_{GaIn}^{exc} = (3311.22 + 914.62X_{Ga})X_{Ga}(1 - X_{Ga})$		— [52]
GaSn	3636.31	- 394.31	— [53]
	3369.7 + 0.03854 (T/K)	528.9 - 0.1145 (T/K)	— [54]
	$\Delta H_{GaSn}^{exc} = (893 + 124X_{Sn})X_{Sn}(1 - X_{Sn})$		— [55]
InSn	- 828.54 + 0.76018 (T/K) - 0.1211767 (T/K) ln[(T/K)]	- 115.59 to 1.39997 (T/K)	— [56]
	- 711 - 1.6934 (T/K)	- 64 to 1.3592 (T/K)	— [57]

Table 4 Density excess of binary sub-alloys

Binary sub-alloy	Predicted mean density excess of the eutectic binary sub-alloys	Predicted concentration and value of maximal density excess of the binary sub-alloys
GaIn	323 K: $-0.28 \pm 0.02\%$ 573 K: $-0.30 \pm 0.02\%$	$X_{\text{In,max}} = 49.3 \pm 0.02 \text{ at.}\%$ ($-0.41 \pm 0.04\%$) $X_{\text{In,max}} = 48.8 \pm 0.02 \text{ at.}\%$ ($-0.44 \pm 0.05\%$)
GaSn	573 K: $-0.17 \pm 0.01\%$	$X_{\text{Sn,max}} = 47.3 \pm 0.03 \text{ at.}\%$ ($-0.34 \pm 0.01\%$)
InSn	573 K: $+0.07 \pm 0.00\%$	$X_{\text{Sn,max}} = 45.6 \pm 0.01 \text{ at.}\%$ ($+0.07 \pm 0.00\%$)

The three excess curves are very close to one another and the comparison with experimental data for 323 K [40–42] and 573 K [40, 42, 43] shows reasonable agreement (Fig. 7a, b).

For the prediction of the density excess of the second binary sub-alloy – GaSn – again two independent sets of interaction parameters [53, 54] and additionally one enthalpy of mixing correlation [55] are utilised. Experimental data are available at 573 K [43–46]. Figure 7c, d) indicate the good agreement between these data and the predicted density excess.

The two sets of interaction parameters [56, 57] used for density prediction of InSn give comparatively low excess values with respect to GaIn and GaSn. The results are again almost identical (Fig. 7e, f). However, neither the sign nor the absolute values match satisfactorily with the experimental data [47–49]. The reason for this could be either that the experimental data is faulty or that the temperature range for which the interaction parameters apply does not match the temperature of this data. Nevertheless, because the atomic geometry of indium and tin as neighbours in the periodic table of elements should be very similar, the excess density, if any, is rather small. Therefore, the further prediction uses the correlations following from [56, 57].

3.3.4 Density of Near-Eutectic Ga–In–Sn Alloy Considering a Possible Excess

Following the approach described above delivers a complex exponential correction function for Eq. 13 (second term, right-hand side). A series expansion of the correction function simplifies the prediction so that the density correlation considering a possible excess reads

$$\rho_{\text{liq,EGaInSn}}^{\text{exc}}(T) = \left[6403.22 \frac{\text{kg}}{\text{m}^3} - 0.6827 \frac{\text{kg}}{\text{m}^3} \frac{1}{\text{K}} (T - T_{\text{m,EGaInSn}}) \right] \times \left[0.9959 - 3.69 * 10^{-6} \frac{\text{kg}}{\text{m}^3} \frac{1}{\text{K}} (T - T_{\text{m,EGaInSn}}) \right] \quad (24)$$

The first factor is identical with Eq. 12 and the second is the correction function. The difference between the complete correlation following from (13) and Eq. 24 falls between $+0.06\%$ at $T_{\text{m,EGaInSn}}$ and -0.02% at 673 K, the highest temperature considered in this study. The correction function is smaller than unity over the entire temperature interval considered.

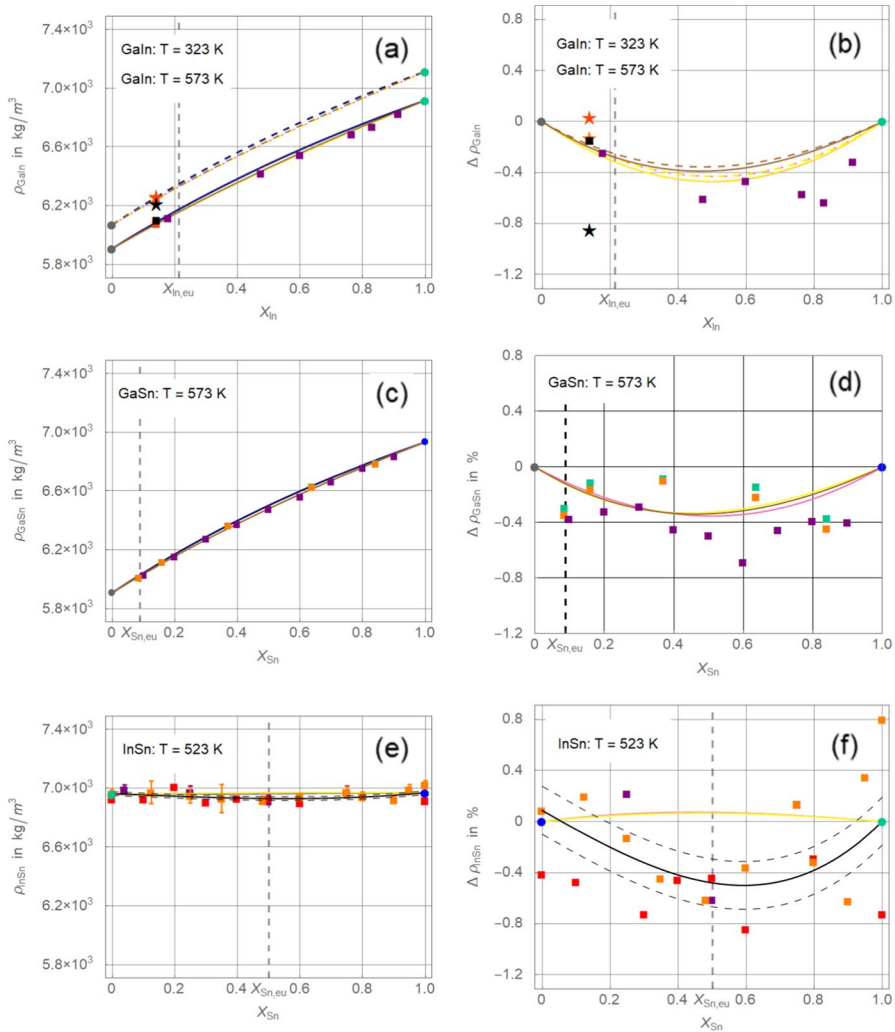


Fig. 7 Density and density excess of binary sub-alloys. Dots at 0 and 1.0 show values for the pure alloying elements (grey Ga, green In and blue Sn). Experimental reference data as given in Table 2. Blue curves (left column) show density without excess. Coloured curves represent modelled densities with excess (left column) and density excesses. Colours according to Table 3

Figure 8 represents the modelling of the liquid density of near-eutectic Ga–In–Sn alloy considering an excess in relation to selected data sets [17–20]. The excess model delivers densities smaller than Eq. 12, which seems plausible. The difference is about -0.41% at $T_{mEGaInSn}$ and about -0.48% at 673 K. These numbers are similar to the values of the maximal density excess of the binary sub-alloys GaIn and GaSn (Table 4). Based on this finding, one may hypothesise that the predicted excess is mainly due to the dissimilarity of the Ga atoms, on

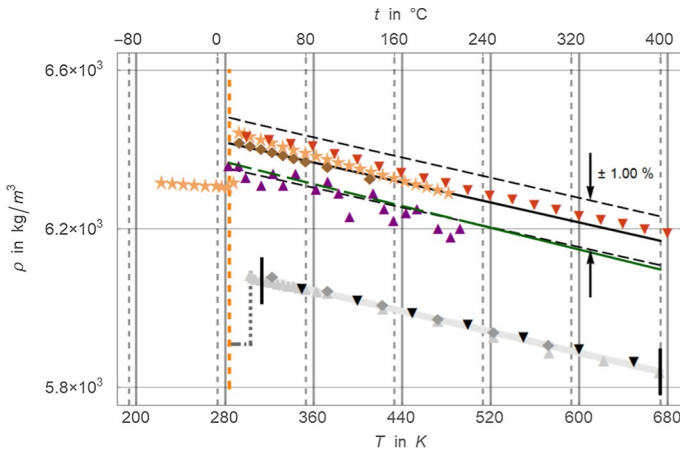


Fig. 8 Modelling of liquid density of near-eutectic Ga–In–Sn alloy considering a possible excess. Symbols according to Table 1. Full black line identifies fitting function (3) $\pm 1\%$. Green curve indicates modelling according to Eq. 24

the one side, and the In and Sn atoms, on the other. The results of Eq. 24 are at the lower one percent border of the fitting function (9). Interestingly, they are in reasonable agreement with the data by Plevachuk et al. [17].

3.4 Thermal Expansion Coefficient and Possible Liquid-to-Liquid Crossover

The study discusses, based on the experimental data and the modelling approaches, the thermal expansion coefficient and a possible liquid-to-liquid crossover proposed by Wang et al. [18].

Figure 9 shows the thermal expansion coefficient derived from three experimental data sets [18–20]. The inevitable density gradients are predicted as linear difference quotients of two consecutive experimental data points without any curve fitting. Additionally, Fig. 9 shows the $\beta(T)$ correlation given by Plevachuk et al. [17] and the correlations following from Eqs. 2 and 8 for the solid and from Eqs. 3, 12 and 24 for the liquid alloy. Data sets not shown scatter significantly due to numerical differentiation.

The expansion coefficient resulting from the fit of the solid-state data (2) is in excellent agreement with the experimental data. The estimate based on atomic volumes of the alloying elements Eq. 8, however, matches only in the mean. The mathematical reason is the nearly zero curvature of this function. The physical background might be the lack of an appropriate correlation for the density of solid gallium.

The correlation of the thermal expansion coefficient following from Plevachuk's density function [17] is in good agreement with the majority of the experimental data in a temperature range between $T_{m,EGaInSn}$ and 500 K. As any other model, it has a weak positive slope. The atomic volume correlation (12) and the correlation considering a possible excess (24) are very close together and match reasonably with the Wang data [18], especially in the higher temperature range.

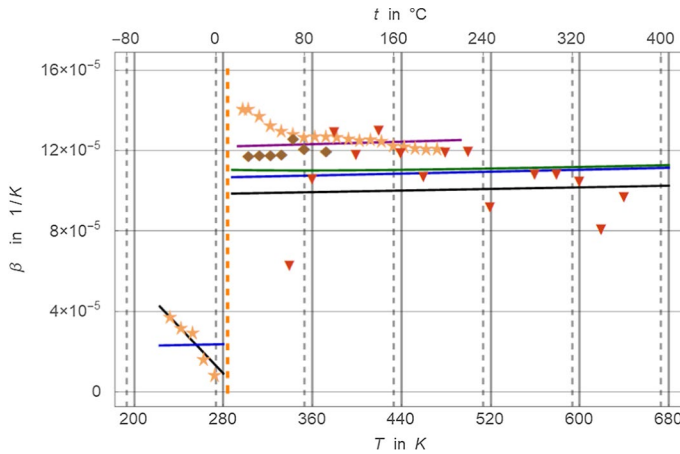


Fig. 9 Thermal expansion coefficient based on experimental data and on modelling approaches. Black for Eqs. 2, 3, blue for Eqs. 8, 12, green for Eq. 24, and purple for Plevachuk et al. [17]

The existence of liquid-to-liquid crossover regions is controversially discussed [58]. One possible cause of such a crossover could be a liquid-to-liquid phase transition, which is accompanied by a density change. Experimental and numerical results on this phenomenon are rare. None of the above models consider such a transition. Furthermore, only one experimental data set shows rudiments of such a behaviour [20].

Figure 10 represents an enlargement of Fig. 9. The distribution of the thermal expansion has three distinct regions. Between the melting point and about 350 K, the values fall monotonically. From 350 to 415 K, a first plateau appears with a β -value of about $12.5 \times 10^{-5} \text{ K}^{-1}$. A second plateau appears at about 450 K with a

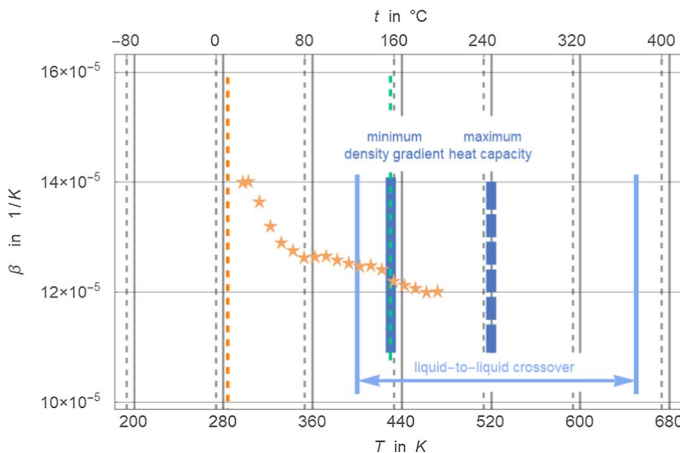


Fig. 10 Thermal expansion coefficient based on experimental data [20] (enlargement of Fig. 9). Vertical broken lines identify melting temperatures of near-eutectic Ga–In–Sn alloy (orange) and indium (green). Borders of the liquid-to-liquid crossover (vertical light blue lines), local minimum of density gradient (bold vertical blue line), and local maximum of heat capacity (bold vertical broken blue line) as described by Wang et al. [18]

slightly smaller β -value of $12.0 \times 10^{-5} \text{ K}^{-1}$. The change between the first and the second plateau marks an inflection point at 430 K. This value coincides reasonably with the minimum of the density derivative of the experimental data by Wang et al. [18]. Surprisingly, this value is in close agreement with indium's melting point $T_{m,\text{In}} = 429.7485 \pm 0.00034 \text{ K}$ [59].

3.5 Recommended Values

Due to the small number of experimental data available for the solid state and the limited applicability of the estimate based on the atomic volumes of the alloying elements, it is recommended to use Eq. 2 as the best model currently available for solid near-eutectic Ga–In–Sn alloy. This correlation holds between 223.15 and 283.15 K (-50 to 10 °C).

The amount of data for the liquid state is significantly larger. All data fit into an error band of $\pm 2\%$. A linear fitting correlation Eq. 3 describes, with the exception of two data sets, all values within an error band of $\pm 1\%$. The estimate based on the atomic volumes is in close agreement with this linear fitting correlation. The second model considering an excess shows a resulting correlation with values about 1% below the fitting correlation. Based on these findings, the fitting correlation still seems to be the best choice for the liquid state of near-eutectic Ga–In–Sn alloy in the temperature interval $T_{m,\text{EGaInSn}} < T < 680 \text{ K}$ (400 °C).

4 Conclusion

Three approaches to describe the density of the solid and the liquid state of near-eutectic gallium-indium-tin alloy are analysed. While the first approach approximates the experimental data using polynomials, the second method utilises the linear combination of the atomic volumes of the pure constituents, weighted by their molar fractions, to model the density. The third approach, a correction function considering a possible excess, is also developed.

The study concludes that, given the recent availability of experimental data and their accuracy, the fitting polynomials are the most reliable models. The difficulties related to the modelling of density and density excess are manifold. Among them is the lack of high accuracy thermophysical properties for the alloying partners. In view of the potential importance of heat transfer based on liquid metals, this gives rise to new research tasks. Including the need for more data on the solid state of near-eutectic Ga–In–Sn alloy. To answer the questions about whether a density excess and liquid-to-liquid crossovers exist, highly accurate high temperature data are urgently needed.

Acknowledgements The Bundesministerium für Wirtschaft und Klimaschutz der Bundesrepublik Deutschland supports the study financially under the research grant 49MF200081. The author thanks Maria José V. Lourenço and Carlos Nieto de Castro (University of Lisbon, Portugal) for the fruitful discussions that supported this work.

Author Contributions M.H.B conceived and authored the paper.

Funding The author has no competing interests to report. The Bundesministerium für Wirtschaft und Klimaschutz der Bundesrepublik Deutschland supports the study financially under the research Grant 49MF200081.

Declarations

Conflict of interest The un-expanded correlations for Eqs. 8 and 24 are available upon request from the author.

References

1. The European Green Deal (europa.eu)
2. A. Heinzl, W. Hering, J. Konys, L. Marocco, K. Litfin, G. Müller, J. Pacio, C. Schroer, R. Stieglitz, L. Stoppel, A. Weisenburger, T. Wetzel, *Energy Technol.* (2017). <https://doi.org/10.1002/ente.v.5.710.1038/s41467-019-11823-4>
3. M.K. Akbari, S. Zhuyikov, *Nat. Commun.* (2019). <https://doi.org/10.1038/s41467-019-11823-4>
4. G. Bo, L. Ren, X. Xu, Y. Du, S. Dou, *Adv. Phys.* (2018). <https://doi.org/10.1080/23746149.2018.1446359>
5. M.M. Sarafraz, M.R. Safaei, M. Goodarzi, B. Yang, M. Arjomandi, *J. Heat Mass Transfer* (2019). <https://doi.org/10.1016/j.jheatmasstransfer.2019.05.057>
6. T. Hao, H. Ma, X. Ma, *J. Heat Transfer ASME* (2019). <https://doi.org/10.1115/1.4043620>
7. R.R. Riehl, M.H. Buschmann, *Appl. Therm. Eng.* (2024). <https://doi.org/10.1016/j.applthermaleng.2023.121413>
8. M.J.V. Lourenço, F.J.V. Santos, V.M.B. Nunes, M. Alves, C.A. Nieto de Castro, R. Mondragón, L. Hernández, R. Künanz, C. Hanzelmann, S. Feja, M.H. Buschmann, *Thermophysical Properties of Eutectic Gallium-Indium-Tin Alloy Revised*, 20th Meeting of the International Association for Transport Properties, Lisbon (Portugal) July 9th 2022
9. M.J.V. Lourenço, M. Alves, J.M. Serra, C.A. Nieto de Castro, M.H. Buschmann, *The Thermal Conductivity of Near-Eutectic Galinstan (Ga_{68.4}In_{21.5}Sn₁₀) Molten Alloy*, *J Thermophysics*, (2023) submitted
10. P.É.L. de Boisbaudran, *Alliages d'indium et de gallium*, (1878) 701–703.
11. H. Spengler, *Z. Metall.* **46**, 464–469 (1955)
12. D.S. Evans, A. Prince, *Met. Sci.* **12**, 411–414 (1978)
13. A. Koh, S. Chun, W. Hwang, P.Y. Zavalij, G. Slipher, R. Mrozek, *Materialia* (2019). <https://doi.org/10.1016/j.mtla.2019.100512>
14. Q. Yu, Q. Zhang, J. Zong, S. Liu, X. Wang, X. Wang, H. Zheng, Q. Cao, D. Zhang, J.Z. Jiang, *Appl. Surf. Sci.* (2019). <https://doi.org/10.1016/j.apsusc.2019.06.203>
15. V.Y. Prokhorenko, E.A. Ratushnyak, B.I. Stadnyk, V.I. Lakh, A.M. Koval, *High Temp.* **8**, 374–378 (1970)
16. L.L. Migai, N.Y. Mikhailov, N.L. Perlova, M.A. Pokrasin, V.V. Roshchupkin, A.I. Chernov, *Russ J Phys Chem* (1981) 2701–2703
17. Y. Plevachuk, V. Sklyarchuk, S. Eckert, G. Gerbeth, R. Novakovic, *J Chem Eng Data* (2014, 2015) <https://doi.org/10.1021/je400882q>
18. X. Wang, Q. Yu, X. Wang, Z. Dai, Q. Cao, Y. Ren, D. Zhang, J.Z. Jiang, *J. Phys. Chem* (2021). <https://doi.org/10.1021/acs.jpcc.1c00370>
19. T. Laube, F. Emmendorfer, B. Dietrich, L. Marocco, Luca, T. Wetzel, *KIT* (2021) <https://publikationen.bibliothek.kit.edu/1000140052>
20. Geratherm priv. Communication (2010)
21. CRC Handbook of Chemistry and Physics, 86th edn. (CRC Press, Boca Raton, 2006)
22. A. Burdakin, B. Khlevnoy, M. Samoylov, V. Sapritsky, S. Ogarev, A. Panfilov, G. Bingham, V. Privalsky, J. Tansock, T. Humpherys, *Metrologia* **45**, 75–82 (2008). <https://doi.org/10.1088/0026-1394/45/1/011>

23. R.L. Orr, H.J. Giraud, R. Hultgren, Third Technical Report Contract No. Nonr-222(63) (1961) University of California, Berkeley California011
24. V.M.B. Nunes, M.J.V. Lourenço, F.J.V. Santos, C.A. Nieto de Castro, *J Thermophys* (2010). <https://doi.org/10.1007/s10765-010-0848-z>
25. V.M.B. Nunes, C.S.G.P. Queirós, M.J.V. Lourenço, F.J.V. Santos, C.A. Nieto de Castro, *J. Thermophys.* (2018). <https://doi.org/10.1007/s10765-018-2388-x>
26. D.D. Williams, R.R. Miller, *New Compounds* (1950) 3821
27. L. Wang, A. Xian, H. Shao, Density measurement of liquid indium and zinc by the c-ray attenuation method. *High Temp.* (2003/2007) 35/36 659–665
28. S.V. Stankus, R.A. Khairulin, *High Temp.* (2006). <https://doi.org/10.1007/s10740-006-0048-5>
29. M.J. Assael, I.J. Armyra, J. Brillo, S.V. Stankus, J. Wu, W.A. Wakeham, *J. Phys. Chem. Ref. Data* (2012). <https://doi.org/10.1063/1.4729873>
30. V.Y. Kezik, A.S. Kalinichenko, V.A. Kalinitchenko, *Z. Metall.* (2003). <https://doi.org/10.3139/ijmr-2003-0019>
31. S. Ayrinhac, M. Gauthier, G. Le Marchand, M. Morand, F. Bergame, F. Decremps, *J. Phys. Condens Matter* **1–8**, 27 (2015)
32. D.K. Belashchenko, *Russ. J. Phys. Chem. A* (2021). <https://doi.org/10.1134/S0036024421110054>
33. M.J. Assael, A.E. Kalyva, K.D. Antoniadis, R.M. Banish, I. Egry, J. Wu, E. Kaschnitz, W.A. Wakeham, *J. Phys. Chem. Ref. Data* (2010). <https://doi.org/10.1063/1.3467496>
34. Y. Liu, Y.H. Liu, X.P. Su, *CALPHAD* (2020). <https://doi.org/10.1016/j.calphad.2019.101690>
35. B. Predel, A. Emam, *Mater. Sci. Eng.* (1969). [https://doi.org/10.1016/0025-5416\(69\)90005-6](https://doi.org/10.1016/0025-5416(69)90005-6)
36. Z. Yu, H. Leng, Q. Luo, J. Zhang, X. Wu, K.C. Chou, *Mater. Des.* (2020). <https://doi.org/10.1016/j.matdes.2020.108778>
37. Peter Linstrom (2017), NIST Chemistry WebBook - SRD 69, National Institute of Standards and Technology <https://doi.org/10.18434/T4D303>. Accessed 24 Oct 2023
38. Indium | Metals & Alloys | Products made by Indium Corporation. Accessed 24 Oct 2023
39. S. Sharafat, N. Ghoniem, Summary of Thermo-Physical Properties of Sn, And Compounds of Sn-H, Sn-O, Sn-C, Sn-Li, and Sn-Si And Comparison of Properties of Sn, Sn-Li, Li, and Pb-Li, UCLA-UCMEP-00-31 Report (2000)
40. Q. Yu, X.D. Wang, Y. Su, Q.P. Cao, Y. Ren, D.X. Zhang, J.Z. Jiang, *Phys. Rev. B* (2017). <https://doi.org/10.1103/PhysRevB.95.224203>
41. Q. Xu, N. Oudalov, Q. Guo, H.M. Jaeger, E. Brown, *Phys. Fluids* (2012). <https://doi.org/10.1063/1.4724313>
42. V.Y. Prokhorenko, V.V. Roshchupkin, M.A. Pokrasin, S.V. Prokhorenko, V.V. Kotov, *High Temp.* (2000). <https://doi.org/10.1023/A:1004157827093>
43. R. Predel, A. Emam, *J. Less Common Met.* (1969). [https://doi.org/10.1016/0022-5088\(69\)90008-3](https://doi.org/10.1016/0022-5088(69)90008-3)
44. T. Gancarz, *J. Mol. Liq.* (2017). <https://doi.org/10.1016/j.molliq.2017.06.002>
45. U.R. Kattner, *JOM* (1997). <https://doi.org/10.1007/s11837-997-0024-5>
46. S.V. Stankus, I.V. Savchenko, A.S. Agazhanov, *J. Thermophys.* (2012). <https://doi.org/10.1007/s10765-012-1192-2>
47. J. Pstruś, *Appl. Surf. Sci.* (2013). <https://doi.org/10.1016/j.apsusc.2012.10.098>
48. Z. Moser, W. Gasior, J. Pstruś, I. Kaban, W. Hoyer, *J. Thermophys.* (2009). <https://doi.org/10.1007/s10765-009-0663-6>
49. P.E. Berthou, R. Tougas, *Metall. Trans.* (1970). <https://doi.org/10.1007/BF03037849>
50. D. Jendrzeczyk-Handzlik, P. Handzlik, *J. Mol. Liq.* (2019). <https://doi.org/10.1016/j.molliq.2019.111543>
51. T.J. Anderson, I. Ansara, *J. Phase Equilib.* (1991). <https://doi.org/10.1007/BF02663677>
52. R. Pong, Thermodynamic studies of Ga-In, Ga-Sb and Ga-In-Sb Liquid alloys by solid state electrochemistry with oxide electrolytes PhD-Thesis Lawrence Berkeley National Lab. (LBNL), Berkeley, CA (United States) (1975) <https://doi.org/10.2172/417715>
53. J. Fels, P. Berger, T.L. Reichmann, H.J. Seifert, H. Flandorfer, *J. Mol. Liquids* (2019). <https://doi.org/10.1016/j.molliq.2019.111578>
54. T.J. Anderson, I. Ansara, *J. Phase Equilib.* (1992). <https://doi.org/10.1007/BF02667485>
55. M. Fornaris, Y.M. Muggianu, M. Gambino, J.P. Bros, *Z. Naturforsch.* (1980). <https://doi.org/10.1515/zna-1980-1121>
56. D. Jendrzeczyk-Handzlik, W. Gierlotka, K. Fitzner, *J Chem Thermodynamics* (2009). <https://doi.org/10.1016/j.jct.2008.09.007>

57. T. Miki, N. Ogawa, T. Nagasaka, M. Hino, *Mater. Trans.* (2001). <https://doi.org/10.2320/matertrans.42.732>
58. S. Lan, M. Blodgett, K.F. Kelton, J.L. Ma, J. Fan, X.L. Wang, *Appl. Phys. Lett.* (2016). <https://doi.org/10.1063/1.4952724>
59. G.F. Strouse, *Materials Sci* (2001) <https://api.semanticscholar.org/CorpusID:139617499>

Publisher's Note Springer Nature remains neutral with regard to jurisdictional claims in published maps and institutional affiliations.

Springer Nature or its licensor (e.g. a society or other partner) holds exclusive rights to this article under a publishing agreement with the author(s) or other rightsholder(s); author self-archiving of the accepted manuscript version of this article is solely governed by the terms of such publishing agreement and applicable law.